The N* Program at CEBAF

Ralph Minehart, for the CLAS Collaboration

Department of Physics, University of Virginia, Charlottesville VA 22901, USA.

Abstract. The N* program at CEBAF is reviewed, and some preliminary experimental results are presented to illustrate the quality and capabilities of the CLAS detector.

Contributed to the Workshop on ELectron Nucleus Scattering, held at the Elba International Physics Center(EIPC), at Marciana Marina (Isola d'ELba, Italy), June 22-26, 1998. Published in "Workshop on ELectron Nucleus Scattering", ed. by Omar Benhar, Adelchi Fabrocini, and Rocco Schiavilla, pub. by Edizioni ETS.

The N* Program at CEBAF

Ralph Minehart, for the CLAS Collaboration

Department of Physics, University of Virginia, Charlottesville VA 22901, USA.

Abstract. The N* program at CEBAF is reviewed, and some preliminary experimental results are presented to illustrate the quality and capabilities of the CLAS detector.

1 Introduction

The availability of high intensity CW electron beams at CEBAF with energies up to 6 GeV has renewed interest in investigating the nucleon and its excited states. While Quantum Chromodynamics (QCD) is generally accepted as the correct theory of the strong interaction, a direct derivation of the structure of quark-gluon bound states from QCD is not yet possible. A description in terms of models is still necessary, but these should be consistent with QCD to as great an extent as possible. Several models keeping with this spirit have been studied. At a minimum, comparisons with experiment can be used to test the range of validity of a model, but at a deeper level it may be possible to test the role played by fundamental features of QCD in bound systems.

The constituent quark model (CQM) [1] has enjoyed a number of successes. In this model much of the dynamical complexity of low energy QCD is hidden in spatially extended, colored, spin 1/2 quasi-particles consisting of bare quarks surrounded by a cloud of quark-antiquark pairs. The mass of the constituent quark is approximately 1/3 of the nucleon mass. Confinement is imposed by the use of an effective potential, such as a harmonic oscillator. With this independent quark model the bound states are members of an SU(6)xO(3) group. Residual interactions between the constituent quarks mix states specified by the confinement potential resulting in significant mass shifts. The choice of the residual interactions affects both static properties and transitions between states. In its original form the constituent quarks were treated non-relativistically, even though the constituents have relativistic energies. Relativistic treatments, however, have not resulted in major changes in the predictions of the baryonic properties. It is quite remarkable that the constituent quark mass required by the model turned out to be consistent with a dynamical quark mass of 315 $\pm$15 MeV arising from chiral symmetry breaking in non-perturbative QCD [2].

Bag models have also been extensively studied. Here the quarks and gluons are confined inside an impenetrable boundary. Variations, such as the addition of a pion cloud around the core, or the addition of mesons inside the bag, have been used to make the model more consistent with the chiral

properties of QCD. The soliton model of the nucleon, originally proposed by Skyrme, is also interesting, particularly because it has been identified with a large N_c approximation to QCD.

In addition to the use of static baryonic properties to test the models, the coupling of the baryonic states to the electromagnetic fields are accessible both to experimental measurement and to model calculations. The electromagnetic interactions are sensitive both to details of this structure and the coupling mechanisms. Measurements can be made over a range in Q^2 extending from the real photon point to several $(GeV/c)^2$. With the large kinematical region covered by the CEBAF Large Acceptance Spectrometer (CLAS), and the capability of operating at luminosities up to $10^{34} cm^{-2} s^{-1}$, it will be possible to obtain data of high statistical accuracy permitting extraction of small components in the partial wave content of the transitions. Characteristic isospin properties of different resonances can be exploited by using both proton and deuteron targets. To this end, an extensive experimental effort, the N* program, is in progress at Thomas Jefferson Laboratory. Individual experiments are listed in Table 1.

2 The N* Program

Excitation of the nucleon to an intermediate resonant state, N*, in the reaction, $e + p \rightarrow e' + N^*$, followed by decay of the N^* to a nucleon and a meson is a major contribution to the single meson electro-production reactions, $e + p \rightarrow e' + p + \pi^0$, $e + p \rightarrow e' + \pi^+ + n$, or $e + p \rightarrow e' + p' + \eta$. The electron nucleon interaction is mediated by a space-like virtual photon that probes the spatial and spin structure of the transition at the quark-gluon level. At high Q^2 the small distance behavior of the quark-gluon confining interaction is probed. Experimentally, these reactions are attractive, since kinematically complete measurements are possible.

Assuming invariance under the time-reversal and parity operators, electroproduction of a pseudo-scalar meson on a nucleon can be expressed in terms of 6 independent complex helicity amplitudes, functions of Q^2, and the invariant mass, W, of the hadronic part of the final state. Measurements of the pion angular distributions identify the spins of the intermediate resonances contributing to the reaction. With an unpolarized beam and target only four response functions can be measured. With a polarized beam and target, additional observables can be measured. Polarization asymmetries are a sensitive method for measurement of small amplitudes through their interference with large amplitudes that dominate the unpolarized cross sections.

The N* program will address the following questions:

1. What is the basic symmetry of the light quark baryons. The SU(6) x O(3) symmetry of the constituent quark model is not the only possibility. A variant of the constituent quark model, the quark-diquark model, can also describe the observed light quark baryon spectrum, and does so with

Table 1. CEBAF Experiments focussing on N* Physics

CEBAF Exp.	Reaction	Q^2 Range	Physics Focus
E-89-037	$ep \to e'p\pi^0$, $e'n\pi^+$,	≤ 4	
	$ed \to e'p\pi^- p_s$	≤ 4	$\Delta(1232)$:
E-94-014	$ep \to e'p\pi^0$	4	Determination of
E-89-042	$ep \to e'p\pi^0$, $e'n\pi^+$	≤ 2	multipoles, M_{1+}, E_{1+}, S_{1+}
E-91-011	$ep \to e'p\pi^0$	1	in large Q^2 range
E-94-003	$ep \to e'p\pi^0$, $e'n\pi^+$	≤ 4	
E-89-038	$ep \to e'p\pi^0$, $e'n\pi^+$,	≤ 4	$P_{11}(1440)$, $D_{13}(1520)$,
	$ed \to e'p\pi^- p_s$	≤ 4	$F_{15}(1680)$, gluonic baryons
E-93-036	$ep \to e'p\pi^0$	≤ 2	
E-93-006	$ep \to e'N\pi\pi$	≤ 2	$S_{31}(1620)$, $D_{33}(1700)$, $D_{15}(1700)$ Missing $\|q^3>$ states, I=1/2, 3/2
E-91-024	$ep \to e'p\omega$	≤ 1	Missing $\|q^3>$ states, I=1/2
E-89-039	$ep \to e'p\eta^0$	≤ 4	$S_{11}(1535)$, $P_{11}(1710)$
E-91-002	$ep \to e'p\eta^0$	4 - 7	High Q^2
E-94-005	$ep \to e'\Delta^{++}\pi^-_{soft}$	≤ 3	$G_A^{\Delta}(Q^2)$, Axial Vector F.F.
E-91-038	$\gamma p \to \eta p$, $\eta' p$	0	$S_{11}(1535)$, $P_{11}(1710)$
E-94-103	$\gamma p \to \pi N$	0	Higher mass resonances
E-93-033	$\gamma p \to p\pi^+\pi^-$	0	Missing states
E-94-109	$\gamma p \to p\rho^0, n\rho^+$	0	Missing states

fewer degrees of freedom so that the number of predicted but unobserved states is smaller. Other models, such as the bag models and skyrmion models have different symmetries.

2. How are gluon degrees of freedom manifested? The success of the CQM indicates that the gluon degrees of freedom seem to be frozen out. Do the gluons have an effect on the internal structure of the known states? If so, what fraction of the angular momentum is related to the gluon degrees of freedom?

With electron energies up to 6 GeV it is possible to explore W masses up to approximately 3 GeV and in a range of Q^2 extending from about 0.3 $(GeV)^2$ up to the order of 6 $(GeV)^2$ for $W < 2$ GeV. For the measurements dicussed here, the maximum beam energy was 4 GeV.

The N* group proposes

1. to measure all accessible processes relevant to decays of N* resonances.

2. to extract the photo-coupling helicity amplitudes, $A_{\frac{1}{2}}$, $A_{\frac{3}{2}}$, and $S_{\frac{3}{2}}$, from the nucleon ground states (n,p) to N* over as large a range in W and Q^2 as practicable. The A's apply to transverse photons and S applies to longitudinal photons.
3. to take advantage of the isospin content of the virtual photon to measure reactions with different isospin content (e.g. $\gamma_v p \to p\pi^0$, $\gamma_v p \to n\pi^+$, and $\gamma_v n \to p\pi^-$), thereby improving the experimental separation of resonant states with different isospin (1/2 or 3/2).
4. to measure the angular distribution of the final state hadrons, which is directly related to the spin of the intermediate resonance state.
5. to analyze resonance production on polarized proton and neutron targets. The measurement of polarization observables provides access to small amplitudes through their interference with dominant amplitudes.

With the high luminosity of the CLAS, the collaboration expects to measure the order of 10^9 events.

Some examples of the questions that can be addressed by the N* program are discussed below. A more complete review may be found in Burkert [3].

The transition $\gamma_v + p \to P_{33}(1232)$, has evoked many theoretical studies. The transition is usually described in terms of the electromagnetic multipoles, M_{1+}, E_{1+}, S_{1+}, and the data require a small, but certainly not zero, electric dipole component, and possibly a longitudinal contribution as well. In the quark model a non-zero value of the ratio $R_{EM} = E_{1+}/M_{1+}$ is usually cited as evidence for a tensor component in the residual effective forces between quarks giving rise to a quadrupole deformation of the nucleon and the Δ. A static deformation of other nucleon resonances would also in principle exist, but so far the experimental evidence is limited to the NΔ transition. Model calculations incorporating a tensor interaction produced by residual one-gluon exchange have yielded a non-zero value for E_{1+}, although there has been a tendency for an accompanying increase in the discrepancy between the calculated and measured magnetic dipole amplitude. Relativistic corrections to the CQM can produce significant alterations to the ground-state wave functions, but they are still too small to account for the measured ratio. Buchmann et al. [4] have studied the role of exchange currents in the transition itself, finding that their effects can be more important than the D state admixtures produced by one-gluon exchange. They obtain E2/M1=-3.5% for real photons. In this model, the N-Δ transition proceeds through the spin-flip of two quarks (e.g. two unpaired spin 1/2 quarks both switch to spin -1/2).

This transition has also been studied in the framework of other models. The chiral bag model predicts an oblate deformation of the nucleon and the Δ because the pion tends to couple at the poles of the nucleon spin. The pion cloud surrounding the core also contributes to the deformation [5]. Kumano [6] has shown that the pion contribution may exceed the contribution from the core deformation. Examples of calculations with other models are numer-

ous, including calculations with the cloudy bag model [7], light-front CQM calculations [8], and calculations in the framework of the Skyrme model [9]. Model calculations of the longitudinal transition have also been carried out [10], [11].

At high enough Q^2 the transition should be described by perturbative QCD, which predicts that $R_{EM} = 1$, but where the perturbative behavior sets in is still an open question.

Both photo-production [12] and electro-production data [13] show that R_{EM} is very small, but not zero, as indicated in Fig. 1, which includes recent data from CEBAF Exp. 94-013 [14] in Hall C. These measurements show that S_{1+} as well as E_{1+} remain small out to Q^2 of 4 $(GeV)^2$. The CLAS measurements will provide detailed data of very high statistical quality over a range in Q^2 from 0.3 to 4 $(GeV)^2$ for the reaction $\gamma_v p \to p\pi^0$. Measurement of the momenta of the charged electron and proton in the final state, in conjunction with the missing mass technique, makes it possible to define the reaction kinematics completely. The restriction of the proton direction inside a narrow cone centered on the q-vector simplifies the experiment. The missing mass technique can also be used in the measurement of the isospin related reaction $\gamma_v p \to n\pi^+$. In the past this reaction has not been well studied because of the experimental complications associated with the lack of constraint in the pion directions. The CLAS detector will provide the first data on this reaction with nearly complete angular coverage, over a large Q^2 region, and with statistical accuracy comparable to the data for $\gamma_v p \to p\pi^0$.

The second resonance region is dominated by two states, $D^+_{13}(1520)$, and $S^+_{11}(1535)$, both of which are members of the $\{70, 1^-\}_1$ in the SU(6)xO(3) group and have therefore the same spatial wave functions. The Q^2 dependence of the transition to the $D^+_{13}(1520)$ is frequently characterized by the ratio

$$A_1 = \frac{A^2_{\frac{1}{2}} - A^2_{\frac{3}{2}}}{A^2_{\frac{1}{2}} - A^2_{\frac{3}{2}}}$$

The Q^2 behavior of this ratio was one of the early successes of the quark model, which predicts that $A_1(Q^2 = 0) = -1$ while $A_1(\text{large } Q^2) \approx 1$. However, detailed comparisons with models require a more accurate and more complete data set than presently exists. The detailed Q^2 behavior, such as the zero crossing point of A_1, is sensitive to models and is different for protons and neutrons ([18]).

The large branching ratio for decay of the $S^+_{11}(1535)$ to the η meson provides an important experimental opportunity. The S-wave η production in the second resonance region, which is just above the threshold at W=1486 MeV, is completely dominated by the $S^+_{11}(1535)$ channel. The transition amplitudes are particularly sensitive to relativistic effects. The observed slow fall-off at high Q^2 could be reproduced by the CQM only with the inclusion of relativistic effects. Sensitivity to the specific parameterization of the con-

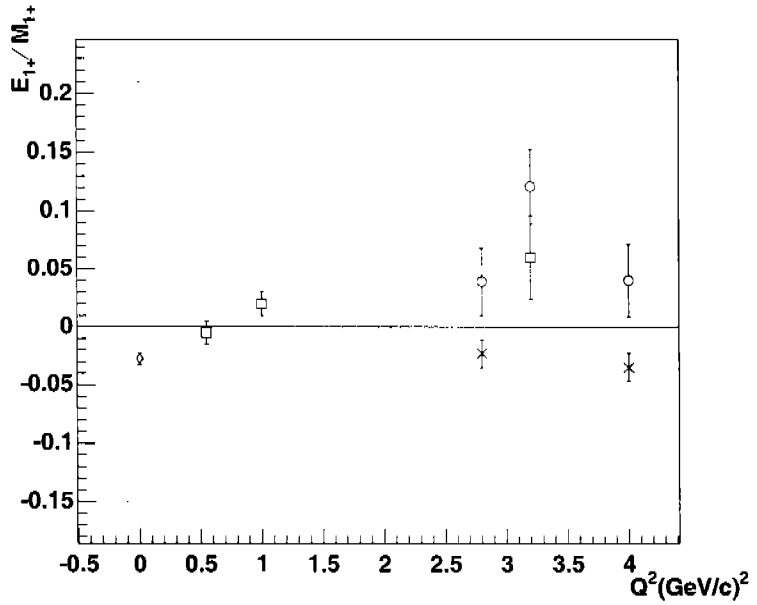

Fig. 1. R_{EM} for $\gamma N\Delta$. Symbols: squares - ref. [15], open circles - ref.[16], crosses [14], photon point - ref. [17]

fining potential found by Warns [10] reinforces expectations that the N* data will provide insights into the quark-gluon confinement.

In the mass region above the η threshold, the N* program will use ηp and $\eta' p$ decay channels as isospin filters to separate N* from Δ^* data [19] and [20]. The $P_{11}(1710)$, which has a large η decay width, should be experimentally accessible.

A test of the spin structure of the transitions is provided by the Q^2 dependence of the ratio $A_{\frac{1}{2}}(1520)/A_{\frac{1}{2}}(1535)$. The comparison of the experimental behavior of this ratio with the predictions of the quark model shown in Fig. 2 indicates a possible large discrepancy at the highest measured Q^2. Whether this discrepancy indicates a serious failing of the CQM requires verification by more complete data.

Another interesting test of the SQTM is provided by the prediction that the radiative transitions from $\{56, 0^+\}$ ground state to $\{70, 1^-\}$ excited states can be described in terms of three amplitudes. Data for the transitions to the $S^+_{11}(1535)$ and $D^+_{13}(1520)$ states can then be used to predict the transition amplitudes to all the other states in the $\{70, 1^-\}$ group. Although the existing data are not in disagreement with these predictions, they are neither sufficiently accurate nor complete enough for a significant test.

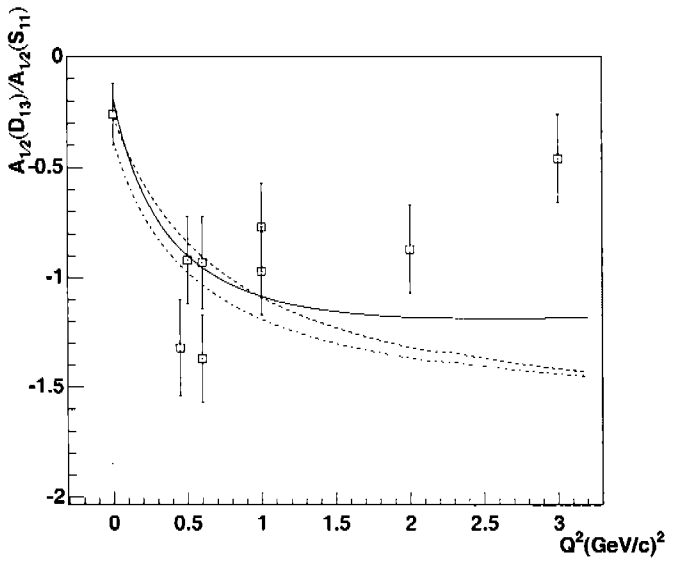

Fig. 2. Q^2 dependence of the ratio $A_{\frac{1}{2}}(1520)/A_{\frac{1}{2}}(1535)$. The curves are from ref. [18]

Some interesting puzzles are associated with the Roper resonance, the $P_{11}(1440)$, which is clearly seen in pion scattering and in photo-production, but has proved elusive in electro-production. In the SU(6) x O(3) group the Roper is a radial excitation with L=0. The quark models using a one-gluon exchange residual interaction have had difficulty reproducing the relatively low mass of this resonance. One success of the NRQM is its correct prediction of the observed neutron to proton photo-production ratio of 2/3. At this conference Riska [21] discusses a model that uses exchange of the octet of pseudo-scalar mesons. This model appears to have a number of advantages, one of which is that it gets the proper ordering of the resonant states in a natural way. Glozman and Riska [22] present a number of arguments why the $N - \Delta$ and $\pi - \rho$ mass splittings are not due to one gluon exchange.

The quark model calculations all agree on the value of the transition form factor at Q^2=0, but they are not consistent with the experimentally observed rapid drop in the magnitude of $A_{\frac{1}{2}}$ with increasing Q^2. In fact, this is so rapid that the amplitude is consistent with 0 for $Q^2 > 0.5$ GeV^2. The NRQM on the other hand predicts a significant increase in the magnitude up to Q^2=0.5 GeV^2. To add to the problem, the relativistic quark models yield too small a value for the transition at Q^2=0 to agree with experiment. All quark models predict a large value for the $S_{\frac{1}{2}}$ amplitude while experiments indicate that

this amplitude is consistent with 0. A calculation of Cardarelli et al. [8] using a light-front constituent quark model that generates a large amount of configuration mixing results in a substantial suppression of the helicity amplitudes for both relativistic and non-relativistic calculations. At the photon point their calculation underestimates the transverse proton transition amplitude but agrees with experiment for the neutron. A model that treats the Roper as a gluonic partner of the nucleon has been shown to give the correct Q^2 dependence and the correct neutron/proton ratio.[23]

The SU(6)xO(3) models predict many more resonances than are observed. The "missing resonances" may provide support for the quark-diquark model for the baryons. With fewer degrees of freedom this model predicts fewer states, but it still reproduces the observed baryonic spectrum. Another possible explanation is that many of the higher mass states decouple from the $N\pi$ channel where the bulk of the data have been obtained. Some states are predicted to couple strongly to other channels, such as $p\omega$, $p\rho$, and $\Delta\pi$, or even to γ p , for example. From an experimental point of view, the ωp channel is an attractive candidate because the narrow width of the ω makes it possible to use missing mass techniques for this final state. Moreover, this channel filters out isospin 1/2 states, eliminating contributions from Δ^* states. On the other hand it has the disadvantage of large contributions from diffractive scattering and from $\omega\pi\gamma$ production. Both of these contributions, however, are characterized by forward peaking in the center of mass hadronic decay angle. The angular distribution for a resonance contribution is relatively flat, so its signal would be most prominent at backward angles. Existing data for photo-production [24] are in agreement with a resonant contribution to $\gamma p \rightarrow \omega p$ with a strength roughly in agreement with the NRQM. However, because of the limited angular range probed by the data it is not possible from the data alone to rule out the possibility that the reaction is entirely non-resonant. If the resonant cross section is as large as predicted it should be possible for a significant measurement to be made at the CLAS in a few weeks of running with 4 GeV electrons.

3 CEBAF and CLAS

The CLAS spectrometer was built by a collaboration of physicists from 32 institutions, listed in Table 2. It is based around a toroidal magnetic field generated by 6 super-conducting coils. The six super-conducting coils divide the sensitive region of the detector into six sectors much like the sectors of an orange. Wire drift chambers are used over an angular region from approximately $10^0 < \theta < 140°$ to track charged particles.

Beyond the drift chambers, the CLAS is enclosed with time-of-flight scintillator strips that have a time resolution of 100 ps. The forward region (from 10° to 45°) is instrumented with gas-filled threshold Cerenkov counters and triangular shaped total absorption scintillator/lead shower calorimeters.

Table 2. The CLAS Collaboration

Institution	Institution
Arizona State University	University of New Hampshire
Carnegie Mellon University	Norfolk State University
Catholic University of America	Ohio University
Christopher Newport University	Old Dominion University
University of Connecticut	University of Pittsburgh
Duke University	Rensselaer Polytechnic Institute
Florida International University	Rice University
Laboratoria Nazionali di Frascati, Italy	University of Richmond
Universita di Genova, INFN, Italy	Centre d'Etudes de Saclay, France
George Washington University	University of Texas at El Paso
Inst. of Theor. and Exp. Physics, Russia	Thomas Jefferson Laboratory
James Madison University	University of Virginia
Kyungpook National University, Korea	Virginia Polytechnic Institute
Massachusetts Institute of Technology	College of William and Mary
University of Massachusetts	Yerevan Physics Institute

To minimize the effect of low energy Møller electrons emerging from the target, the target is surrounded by a second toroidal magnet, called the "mini-torus", which uses six room-temperature coils located in the shadows of the coils of the main torus. The CLAS is capable of operation at luminosities up to $L = 10^{34}$ cm^{-2}s^{-1}.

A photon tagging facility upstream from CLAS provides the option to study real photo-production with an incident photon energy resolution of 6 MeV. The tagger operates up to a rate of 10^8 photons per second with photon energies up to 95% of the electron beam energy.

4 Experimental results from the E1 run

The first data were taken in the E1 run in late 1997 and early 1998. Using unpolarized beams of energies of 1.6, 2.4, and 4.0 GeV, the run provided data for most of the experiments listed in Table 1 that do not require polarized beam or target. The target was a 4 cm liquid hydrogen target with thin aluminum entrance and exit windows. The luminosity varied from $(1-4) \times 10^{33}$ cm^{-2}s^{-1}. Some preliminary results of the run are presented here, primarily to illustrate the capabilities of the spectrometer.

4.1 Data reduction

Since an analyzable event must include an electron to establish Q^2 and W, events were triggered by a coincidence between a signal from the Cerenkov counter and the calorimeter in the same sector. To minimize the trigger bias the thresholds for these signals were set low, at levels corresponding to 0.2 photoelectrons in the Cerenkov counter and 300 MeV energy deposited in the calorimeter. The data acquistion rate was limited by the data acquisition system to 350-500 Hz. About 1/4 of the events contained at least one negative track. Continued improvements in data acquisition hardware and software have increased the data acquistion rate to more than 1 kHz.

The tracks through the drift chamber regions are reconstructed by first matching wire hits to a set of 'roads'. Each of the three drift chamber region consists of two sectors. If hits in five of the six sectors fit to a road, a track is calculated by fitting the struck wires by varying the track parameters. Next the track is followed to a time-of-flight counter, which provides the time of arrival of the particle. Electrons are identified by matching negative tracks with the hits in the Cerenkov counter and a shower in the calorimeter. A fiducial cut is used to make sure that the electrons are inside an efficient region of the Cerenkov counter and calorimeter. In addition the energy measured by the calorimeter must match the track momentum.

After selecting events with good electrons, their path length is determined from the hit-based track and this is used with the time of its arrival in the time-of-flight scintillator to calculate the zero time for the event. This zero time is used to calculate the time of flight for any other particles that triggered one of the time-of-flight scintillators. The start time is combined with the signal times for each wire in the drift chamber to calculate a drift time for that wire, and hence the distance of closest approach of the particle to the wire. This allows a re-calculation of the path of the particle, to attain the ultimate spatial and momentum resolution. Although the track reconstruction efficiency is still being improved it is better than 95%.

After reconstruction of the tracks and determination of the momenta, time-of-flight and path length, the mass of the charged particle can be calculated from its velocity and momentum. The mass resolution is illustrated in Fig. 3 where the momentum of positive partices is plotted vs. $\beta = v/c$. The signal to background for resolving bands of π^+ and protons is excellent. Also, the plot shows a band due to deuterons produced in the end caps of the target.

4.2 Inclusive Electron Scattering

Since the events are triggered on a single electron, inclusive electron scattering provides the first check on the detector. In Fig. 4, the invariant mass, M_x, of the missing particle, X, in the reaction, $e + p \rightarrow e' + X$, is plotted for three incident electron energies. The peak at $M_x = 940$ MeV clearly identifies

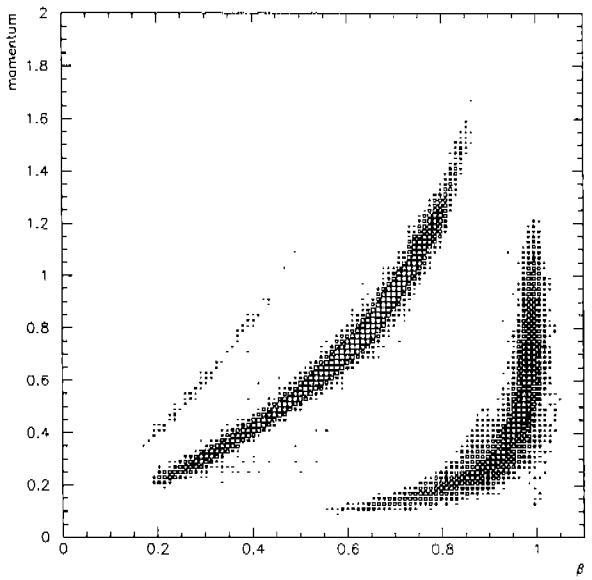

Fig. 3. Momentum vs. β for positive tracks. The size of the box for each bin is proportional to the log of the number of counts.

elastic *ep* scattering. The widths of the elastic peaks are consistent with an electron momentum resolution of 0.5% in the forward region. In the missing mass region above the proton peak the elastic radiative tail and meson production are evident. The meson production is dominated by the $\Delta(1232)$ resonance, and a peak around 1500 MeV clearly indicates production through excitation of resonances in the second resonance region.

4.3 Elastic Scattering Cross Section

Since the cross section is well known, elastic electron scattering provides an excellent check on the calibration and efficiency of the overall system. Fiducial cuts were made to include a volume of the detector where the acceptance is believed to be unity, and the inclusive electron scattering inside this volume was used to calculate the elastic scattering cross section. Preliminary results for one sector with background from the target end-caps subtracted are shown Fig. 5. By comparison of the measured cross section to a calculation using the proton dipole form factor, it can be seen that the preliminary results are correct to within a few per-cent. For the electrons detected inside the fiducial volume, the recoil proton should also be detected. The ratio of the measured inclusive to the measured exclusive elastic scattering cross section shows that

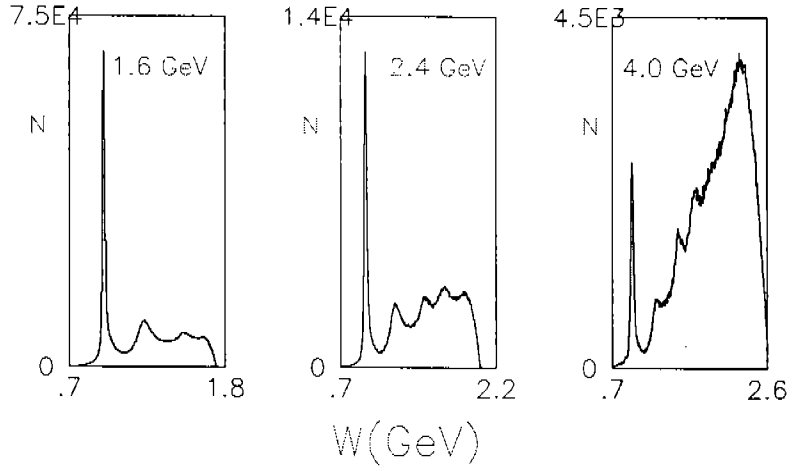

Fig. 4. Invariant hadronic mass for $e + p \rightarrow e' + X$.

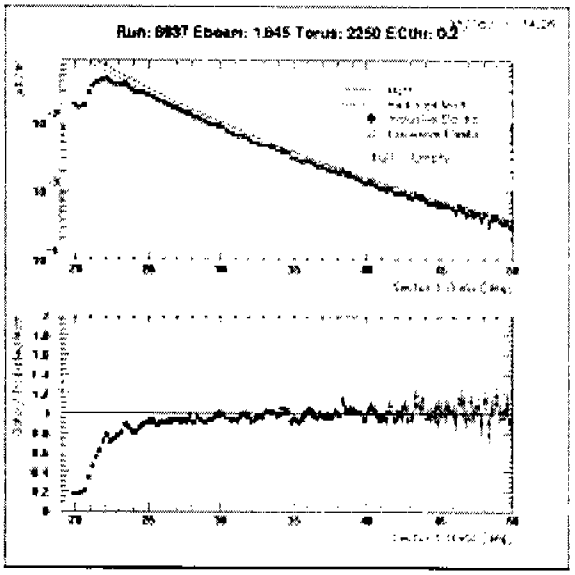

Fig. 5. Cross section for electron elastic scattering compared to the dipole model. Here "inclusive" means that only detection of the electron was required, and "exclusive" means that the recoil proton was also observed.

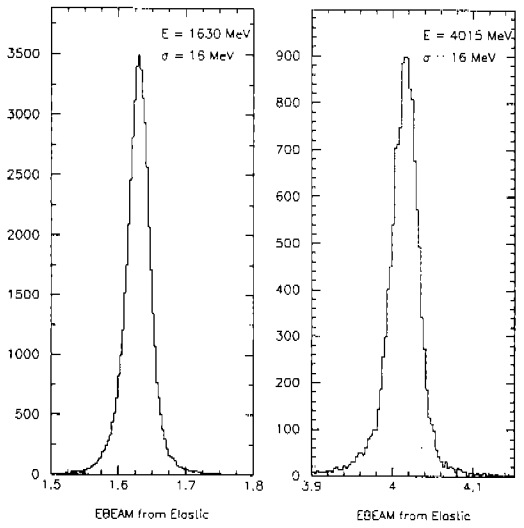

Fig. 6. Beam energy determined from electron and proton angles for elastically scattered electrons.

with the present tracking codes the proton detection efficiency is about 95%. Except for known effects, such as isolated broken wires or bad amplifiers, the six sectors are in excellent agreement with each other.

Detection of both the recoil proton and the electron over-constrains the measurement of elastic scattering. The electron and proton angle by themselves are sufficient to determine the beam energy, according to $E_0/M_p = \cot(\theta_p)\cot(\theta_e/2) - 1$. Plots of the calculated beam energy for data at two of the three employed energies are shown in Fig. 6. The centroids of the peaks are slightly lower than the nominal beam energies. These discrepancies can be explained by a shift of 1.1 mrad in the same direction for both the electron and the proton angle. This small angular error is close to the 1 mrad design goal for the angular resolution of the detector, as are the widths of the peaks which correspond to an angular resolution of approximately 1.5 mrad.

4.4 Analysis of exclusive final states

The goal of our program is to measure resonance contributions to a variety of exclusive final states. Determination of cross sections requires detailed understanding of the combined acceptance function for all the particles in the reaction. At this time we are using simulations to determine the acceptance. Although these studies are not complete, preliminary studies have been car-

ried out with the aid of approximations for which the main disadvantage is the sacrifice of some of the acceptance. To illustrate the data analysis, we can study events with a scattered electron and a single positive particle. From these events we can use the missing mass technique to select the final state, $e' + p' + (\pi^0)$ from the $e'p'X$ data and the final state $e' + \pi^+ + (n)$ from the $e'\pi X$ data.

For data taken at 1.645 GeV, a plot of the square of missing mass for $e'pX^0$ events is shown in the upper half of Fig. 7. Two incompletely resolved peaks are clearly visible near zero mass. The lower peak is due to radiative elastic scattering, $e+p \rightarrow e'+p'+\gamma$, while the upper one is from $e+p \rightarrow e'+p'+\pi^0$. Since the radiative scattering is sharply peaked for photons emitted along the directions of either the incident or scattered electron, it is possible to remove much of the radiative scattering by making cuts in the combined space of missing mass and the direction of the missing momentum. This is illustrated in Fig. 7 where the missing mass spectrum after making these cuts is plotted with asterisks. It is clear that very few pions are removed.

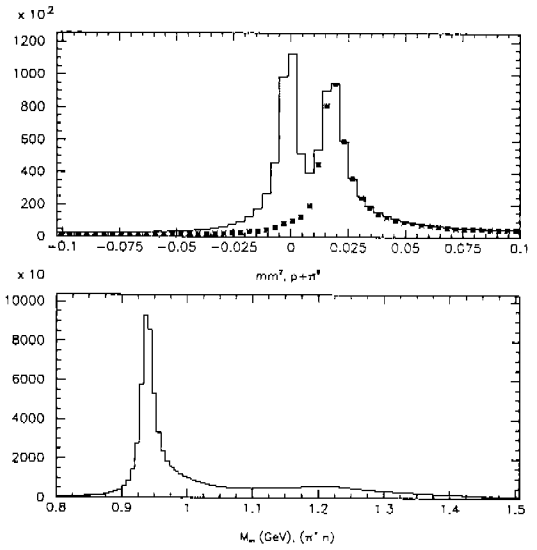

Fig. 7. Upper: Missing mass squared for $ep \rightarrow e'pX^0$. The asterisks show the spectrum after cuts to remove the radiative elastic tail. Lower: Missing mass for $ep \rightarrow e'\pi^+X^0$.

The reaction $ep \rightarrow e'\pi^+n$ has no background from radiative elastic scattering, but the reaction phase space included in the CLAS acceptance is quite

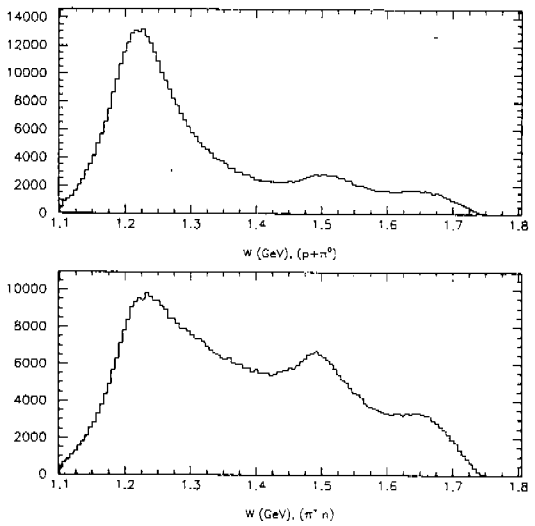

Fig. 8. Resonance spectra for single π^0 (upper) and π^+ (lower) production, with incident beam energy of 1.645 GeV.

different from that for π^0 production since the laboratory direction of the π^+ is unconstrained. Moreover, the consequences of pion decay must be considered. A missing mass plot for events in which only an electron and a π^+ were detected is shown in the lower part of Fig. 7. By making cuts around the neutron peak, the reaction, $ep \rightarrow e'n\pi^+$. can be extracted with rather little background. In this figure one can also see a Δ peak arising from the reaction, $e + p \rightarrow e' + \pi^+ + \Delta^0$.

The spectra of W for the reactions $ep \rightarrow e'p\pi^0$ and $ep \rightarrow e'\pi^+n$ are shown in Fig. 8. Because these spectra are not corrected for the difference in acceptance, a quantitative comparison is not in order. However, the Δ peak is less dominant for π^+ than for π^0 production, as is expected from isospin arguments which require the cross section at the $\Delta(1232)$ peak to be lower by a factor of 2. Background from Born contributions to π^+ production also add to the differences in the two reactions.

Using preliminary calculations of the CLAS acceptance, it is possible to extract cross sections from the data. As an example, the W dependence of the single π^0 production is shown in Fig. 9 along with a plot of the Q^2 behavior for three cuts in W in the the $\Delta(1232)$ resonance region. Because of the preliminary status of the analysis, these cross sections are subject to large systematic uncertainties, of the order of 20%.

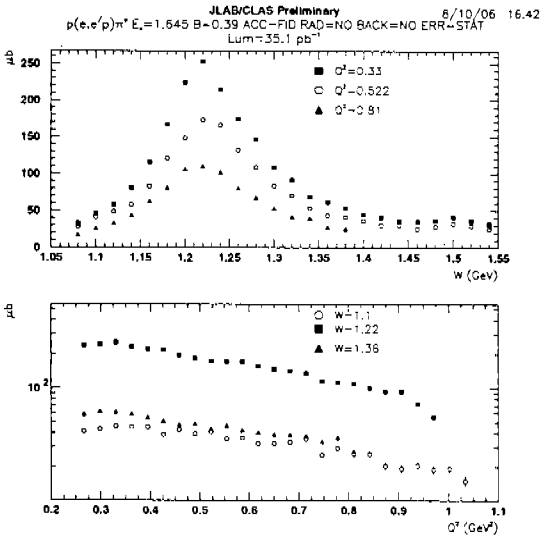

Fig. 9. W and Q^2 dependence of the reaction $e + p \rightarrow e' + p + \pi^0$ in the region of the $\Delta(1232)$.

A number of other reactions listed in Table 1 are being studied at the three energies 1.645, 2.445 and 4.445 GeV, measured. In addition it is also possible to extract K mesons in the data to study production of strange resonances.

5 Conclusions

The N* collaboration expects to obtain statistically precise data on a large number of reactions proceeding through intermediate resonance states. The measurements will extend over Q^2 up to 4 GeV^2 while covering essentially all the phase space for the resonance decays. Preliminary results show that the CLAS is performing at a level close to its design specifications.

Acknowledgments

I would like to thank Cole Smith and Volker Burkert for a critical reading of the manuscript, and emphasize that this paper represents the work of the entire CLAS collaboration.

References

1. N. Isgur and G. Karl, Phys. Letts. **72B**, 109 (1977), Phys. Rev D23, 817 (1981), R. Koniuk and N. Isgur, Phys. Rev. **D21**, 1868 (1980).
2. B.H.J. McKellar, M.D. Scadron, and R.C. Warner, Int. J. Mod. Phys. **A3**, 203 (1988).
3. V. D. Burkert, Electroproduction of Light Quark Baryons, Chapter in "Nucleon Resonance and Nucleon Structure", World Scientific, Ed. G. Miller, (1993).
4. A.J. Buchmann, E. Hernandez, and Amand Faessler, Phys. Rev. **C55**, 448 (1997).
5. L. Heller et al., Phys. Rev. **C35**, 718 (1987).
6. S. Kumano, Phys. Lett. **B214**, 132 (1988).
7. K. Bermuth, D. Drechsel, L. Tiator, J. B. Seaborn, Phys. Rev. **D37**, 89 (1988).
8. F. Cardarelli, E. Pace, G. Salme, S. Simula, Phys. Lett. B371, 7 (1996), Phys. Letters **B397**, 13 (1997).
9. A. Wirzba and W. Weise, Phys. Lett. **B188**, 6 (1987), A. Abada, H. Weigel, H.Reinhardt, Phys. Lett. **B366**, 26 (1996).
10. M. Warns, H. Schröder, W. Pfeil, H. Rollnik, Z. Phys. **C45**, 627 (1990).
11. Z. Li, Y. Dong, W. Ma, Los Alamos Preprint, hep-ph/9409031.
12. Photo-production of the $\Delta(1232)$
13. W. Albrecht et al., Nucl. Phys. **B27**, 615(1971), S. Galster et al., Phys. Rev. **D5**,519 (1972), R. Siddle et al., Nucl. Phys. **B35** (1971), R. D. hellings et al., Nucl. Phys. **B46**, 573 (1972), J. C. Alder et al., Nucl. Phys. **B46**, 573 (1972), K. Bätzner et al., Nucl. Phys. **B75**, 1 (1974).
14. V. V. Frolov et al., submitted to Phys. Rev. Letters.
15. V.D. Burkert and L. Elouadrhiri, Phys. Rev. Lett. **75**, 3614 (1995).
16. I. Aznauryan and S. Stepanyan, private communication.
17. R. Beck et al., Phys. Rev. Lett. **78**, 606 (1997).
18. S. Capstick, Phys. Rev. **D46**, 2864 (1992).
19. CEBAF Proposal 89-043, L. Dennis, H. Funsten (spokespersons)
20. CEBAF Proposal 91-008, B. Ritchie (spokesperson).
21. D. O. Riska, "The effective interaction between constituent quarks and the structure of baryons", Contribution to this conference.
22. L. Ya. Glozman and D.O. Riska, Phys. Rept. **268**, 263 (1996).
23. Z.P. Li, V. Burkert, Z. Li, Electroproduction of the Roper Resonance as a Hybrid State, Preprint CEBAF-PR-91-032 (1991).
    V. Burkert and Zh. Li, Preprint CEBAF-PR-92-017 (1992).
24. J. Ballam, et al., Phys. Rev. **D7**, 3150 (1973), P. Joos, et al., Nucl. Phys. **B122**, 365 (1977).